Tumor functional sphericity from PET images: prognostic value in NSCLC and impact of delineation method

Supplemental material

PET segmentation methods

Fixed thresholds

Thresholds of intensities at respectively 40% (T50) or 50% (T50) of SUV_{max}.

FLAB

FLAB incorporates a fuzzy measure within a Bayesian-based statistical segmentation framework, in order to take into account both noise characteristics and limited spatial resolution of PET images when performing voxels classification in different classes (*e.g.* background or tumor). The parameters (mean and standard deviation of statistical distributions for each class and fuzzy transitions between classes, as well as neighboring voxels spatial correlation) are initialized through a simple fuzzy C-means and are subsequently estimated within an iterative process. FLAB was first proposed with 2 classes only [1] and was subsequently improved to better account for heterogeneous uptake using 3 classes [2,3]. Its robustness and reproducibility was thoroughly evaluated [4–6]. It was also used in PET images with different radiotracers such as FLT [7] or FMISO [8]. Most of these previous studies relied on the user for the choice of 2 or 3 classes. In the present work, an automated detection of the number of classes was implemented so it could be run without user intervention, for a fair comparison with the other methods.

ACO

ACO is a population-based model that mimics the collective foraging behavior of real ant colonies. Artificial ants explore their environment (in the present case the PET volume) in quest for food (the aimed functional volume) and exchange information through iterative update of pheromone quantitative information, which attracts other ants along their path. The food source was initialized by considering the food as a r-radii neighborhood Nr(o) around voxels of intensity 70% of the maximum of the SUV. Unlike global thresholding, local neighborhood analysis is exploited to enhance the spatial consistency of the final volume. After convergence, a pheromone map is obtained with highest density in the estimated volume. The method was initially developed using 2 classes (Fayad et al., 2015).

GARAC

GARAC is a hybrid level-set 3D deformable model driven by both vector field convolution (VFC) edge-based force fields (EBF) [9] and global region-based forces [10]. GARAC exploits both local and dynamic weighting of the EBF term influence according to a blind estimation of its relevance, in order to allow the contour to evolve towards the tumor boundary. EBF can generate centers of divergence [11] that act as impassable barriers preventing the contour to evolve. They are also more sensitive to noise because of their local nature and are thus not well defined everywhere across the PET image domain. In order for the contour to take advantage of global statistics for increased robustness and exploiting the more local

edge information dynamically for increased accuracy around edges [12], the EBF term is locally weighted proportionally to the degree of collinearity between inner and outer net edge forces in the vicinity of each node of the discretized interface. It was observed on training data that the method tends to substantially underestimate volumes (high positive predictive value, low sensitivity). A 1-voxel dilatation of the resulting contour was implemented to improve sensitivity and resulting accuracy.

Table 1

Type of PET images	Associated ground-truth	Details
Synthetic and realistic simulated images	Voxel-based from the simulated object	14 synthetic images (LaTIM, Brest, France) 12 images simulated with GATE [13] (LaTIM, France) 50 images simulated with SIMSET [14] (M. Aristophanous, MD Anderson, USA)
Physical phantom acquisitions	Volumes derived through thresholding of the associated high resolution CT	Different acquisitions of a physical phantom containing 11 zeolites (no cold walls) of various shapes and sizes [15] (E. De Bernardi, Italy). Total of 75 images (6×11 + 3×3).
Clinical images	Digitized reconstructed volumes from histopathology slices.	19 images of head and neck or lung tumors with associated histopathology volumetric measurements [16,17] (J. A. Lee, UCL, Belgium).
Clinical images	Statistical consensus of 3 different manual contours by 3 experts using STAPLE [18].	6 images of lung tumors with consensus of manual delineations by 3 experts [19] (C. Cheze Le Rest, CHU de Poitiers, France).

Table 2. Stratification of patients into three groups using volume and sphericity derived by each segmentation.

Segmentation methods	Stratification using volume and sphericity into three groups						
	Median OS			Hazard ratios between groups			Log-rank p-value
	1st group	2nd group	3rd group	1 *vs*. 2	2 *vs*. 3	1 *vs*. 3	
ACO	41.9 (n=23)	15.4 (n=18)	12.4 (n=46)	2.25	1.32	2.97	**0.0034**
FLAB	41.9 (n=22)	18.4 (n=24)	9.1 (n=41)	1.56	2.19	3.41	**0.0001**
GARAC	30.4 (n=12)	20.2 (n=21)	13.4 (n=54)	1.35	1.92	2.58	0.0152
T50	25.1 (n=20)	23.0 (n=26)	10.5 (n=41)	1.09	2.32	2.54	**0.0011**
T40	25.1 (n=18)	31.3 (n=20)	12.4 (n=49)	0.87	2.59	2.26	**0.0019**

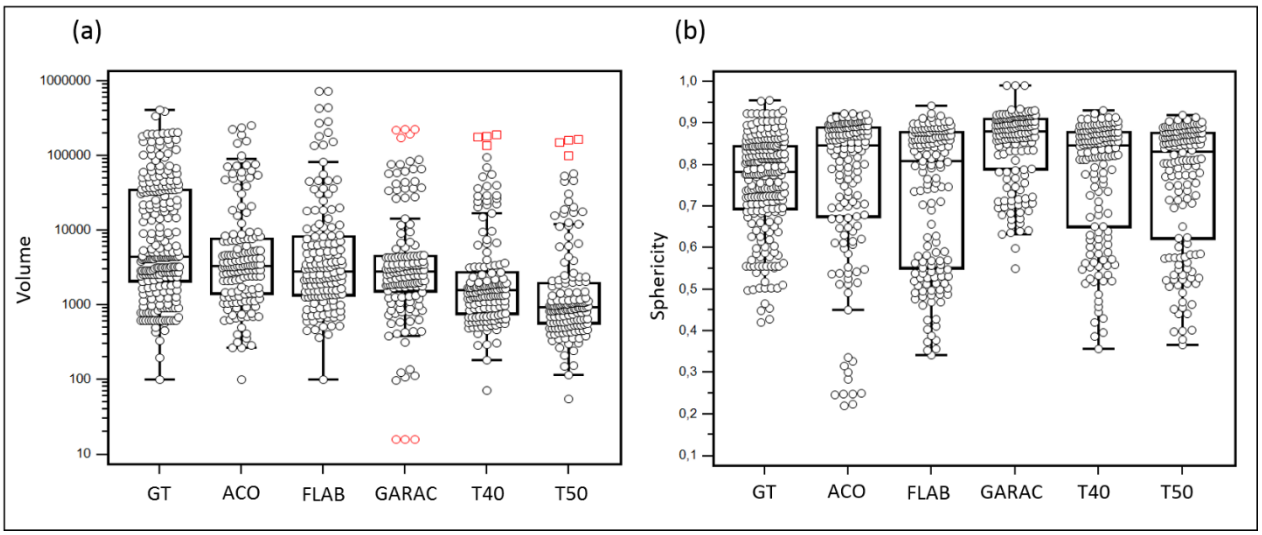

Figure 1: Distributions of volume and sphericity of the first dataset with ground-truth, for the ground-truth and all 5 segmentation methods.

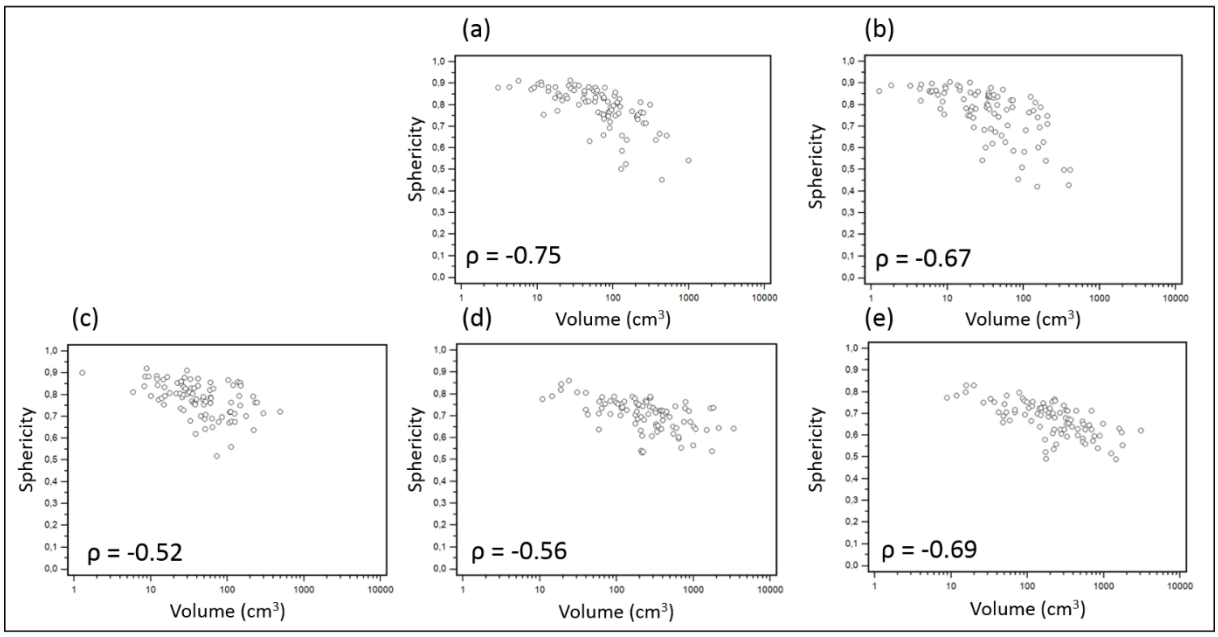

Figure 2: scatter diagrams and Spearman rank correlations (ρ) between volume and sphericity determined by (a) ACO, (b) FLAB, (c) GARAC, (d) T40 and (e) T50, in the 87 NSCLC tumors.

References

1. Hatt M, Cheze le Rest C, Turzo A, Roux C, Visvikis D. A fuzzy locally adaptive Bayesian segmentation approach for volume determination in PET. IEEE Trans Med Imaging. 2009;28:881–93.

2. Hatt M, Cheze-le Rest C, van Baardwijk A, Lambin P, Pradier O, Visvikis D. Impact of tumor size and tracer uptake heterogeneity in (18)F-FDG PET and CT non-small cell lung cancer tumor delineation. J Nucl Med. 2011;52:1690–7.

3. Hatt M, Cheze le Rest C, Descourt P, Dekker A, De Ruysscher D, Oellers M, et al. Accurate automatic delineation of heterogeneous functional volumes in positron emission tomography for oncology applications. Int J Radiat Oncol Biol Phys. 2010;77:301–8.

4. Hatt M, Cheze Le Rest C, Albarghach N, Pradier O, Visvikis D. PET functional volume delineation: a robustness and repeatability study. Eur J Nucl Med Mol Imaging. 2011;38:663–72.

5. Hatt M, Cheze-Le Rest C, Aboagye EO, Kenny LM, Rosso L, Turkheimer FE, et al. Reproducibility of 18F-FDG and 3'-deoxy-3'-18F-fluorothymidine PET tumor volume measurements. J Nucl Med. 2010;51:1368–76.

6. Heijmen L, de Geus-Oei LF, de Wilt JH, Visvikis D, Hatt M, Visser EP, et al. Reproducibility of functional volume and activity concentration in (18)F-FDG PET/CT of liver metastases in colorectal cancer. Eur J Nucl Med Mol Imaging [Internet]. 2012; Available from: http://www.ncbi.nlm.nih.gov/entrez/query.fcgi?cmd=Retrieve&db=PubMed&dopt=Citation&list_uids=22945372

7. Arens AIJ, Troost EGC, Hoeben BAW, Grootjans W, Lee JA, Grégoire V, et al. Semiautomatic methods for segmentation of the proliferative tumour volume on sequential FLT PET/CT images in head and neck carcinomas and their relation to clinical outcome. Eur. J. Nucl. Med. Mol. Imaging. 2014;41:915–24.

8. Henriques de Figueiredo B, Zacharatou C, Galland-Girodet S, Benech J, De Clermont-Gallerande H, Lamare F, et al. Hypoxia imaging with [18F]-FMISO-PET for guided dose escalation with intensity-modulated radiotherapy in head-and-neck cancers. Strahlenther. Onkol. Organ Dtsch. Rontgengesellschaft Al. 2014;

9. Li B, Acton ST. Active contour external force using vector field convolution for image segmentation. IEEE Trans. Image Process. Publ. IEEE Signal Process. Soc. 2007;16:2096–106.

10. Chan TF, Vese LA. Active contours without edges. IEEE Trans. Image Process. Publ. IEEE Signal Process. Soc. 2001;10:266–77.

11. Tauber C, Batatia H, Ayache A. A general quasi-automatic initialization for snakes: application to ultrasound images. IEEE Int. Conf. Image Process. 2005. 2005. p. II-806-9.

12. Jaouen V, González P, Stute S, Guilloteau D, Chalon S, Buvat I, et al. Variational segmentation of vector-valued images with gradient vector flow. IEEE Trans. Image Process. Publ. IEEE Signal Process. Soc. 2014;23:4773–85.

13. Papadimitroulas P, Loudos G, Le Maitre A, Hatt M, Tixier F, Efthimiou N, et al. Investigation of realistic PET simulations incorporating tumor patient's specificity using anthropomorphic models: creation of an oncology database. Med. Phys. 2013;40:112506.

14. Aristophanous M, Penney BC, Pelizzari CA. The development and testing of a digital PET phantom for the evaluation of tumor volume segmentation techniques. Med Phys. 2008;35:3331–42.

15. Zito F, De Bernardi E, Soffientini C, Canzi C, Casati R, Gerundini P, et al. The use of zeolites to generate PET phantoms for the validation of quantification strategies in oncology. Med. Phys. 2012;39:5353–61.

16. Geets X, Lee JA, Bol A, Lonneux M, Gregoire V. A gradient-based method for segmenting FDG-PET images: methodology and validation. Eur J Nucl Med Mol Imaging. 2007;34:1427–38.

17. Wanet M, Lee JA, Weynand B, De Bast M, Poncelet A, Lacroix V, et al. Gradient-based delineation of the primary GTV on FDG-PET in non-small cell lung cancer: A comparison with threshold-based approaches, CT and surgical specimens. Radiother Oncol. 2011;98:117–25.

18. Warfield SK, Zou KH, Wells WM. Simultaneous truth and performance level estimation (STAPLE): an algorithm for the validation of image segmentation. IEEE Trans Med Imaging. 2004;23:903–21.

19. Lapuyade-Lahorgue J, Visvikis D, Pradier O, Cheze Le Rest C, Hatt M. SPEQTACLE: An automated generalized fuzzy C-means algorithm for tumor delineation in PET. Med. Phys. 2015;42:5720.